Akowuah *et al.*
Journal of Electrical Systems and Inf Technol (2023) 10:25
https://doi.org/10.1186/s43067-023-00093-2

Journal of Electrical Systems and Information Technology

RESEARCH Open Access

Ultra-high birefringence with tuneable double zero chromatic dispersion-PCF: a theoretical analysis

Emmanuel Kofi Akowuah[1], Patrick Atsu Agbemabiese[2*] and Alexander Kwasi Amoah[1]

*Correspondence: paagbemabiese@gmail.com

[1] Department of Computer Engineering, Kwame Nkrumah University of Science and Technology, Kumasi, Ghana
[2] Department of Electrical and Electronic Engineering, Koforidua Technical University, Koforidua, Ghana

Abstract

This work presents photonic crystal fibres made up of four hexagonal shape of four rings. Four structures have been designed and configured. The structures show improvement in optical properties consecutively to achieve the optimum configuration. The full vectorial finite-element method is adopted for this work. COMSOL Multiphysics is used for the simulation. The results show a birefringence of 1.308×10^{-2} at 1.55 µm and tuneable double zero dispersion at wavelengths of 0.99 µm and 1.8 µm for *x*-polarisation mode. Also, the chromatic dispersion of − 24.062 ps/km nm and nonlinear coefficient of 30.32 W^{-1} km^{-1} are obtained at a telecommunication wavelength of 1.55 µm. The proposed photonic crystal fibre can be beneficial in nonlinear and supercontinuum applications since photonic crystal fibres of double zero dispersion demonstrate higher power spectral densities than single zero dispersion.

Keywords: Birefringence, Finite-element method, Chromatic dispersion, Confinement loss, Wavelength, Photonic crystal fibres

Introduction

In the telecommunication market today, there are two main fibre optic waveguides. These are the conventional optical fibre and photonic crystal fibre (PCF). The particular applications of PCF have championed the establishment of Blaze photonics in the United Kingdom, Crystal Fibre A/S Denmark and many others for PCF manufacturing. Furthermore, coming-United States, NTT Japan, and Mitsubishi Cable Japan are companies known for producing conventional fibres and, as such, have also jumped into the production of photonic crystal fibre structures (PCFs) [1].

Conventional optical fibres use a solid core, surrounded by cladding. The fibre core has a refractive index higher than the cladding. The core is usually doped to realise a high refractive index contrast. On the other hand, when it comes to PCFs, the core could be either solid, called effective index PCF, or hollow-core, called bandgap guiding PCF [2].

In conventional step-index fibres, very high Birefringence and tuneable chromatic dispersion are challenging to obtain simultaneously. However, these can be achieved in PCF due to the flexibility in design and guiding mechanism. Birefringence of PCFs maintains

the propagation of two orthogonal linear polarisation states over long distances along the fibre.

The contrast between the core and the cladding is higher in PCFs than in conventional step-index fibres. This makes PCFs have higher Birefringence than their traditional step-index counterparts. Birefringence finds applications in fibre lasers, switching, splitting, sensors, telecommunications and supercontinuum generation [3, 4].

Research on PCFs has demonstrated that the core can employ elliptical holes to increase the birefringence [2]. Lee et al. [3] demonstrated recently that a double cladding structure could be used to achieve ultra-high birefringence and a significant negative dispersion. A hybrid cladding can also achieve a birefringence of 10^{-2} [5]. The core of the PCF can be designed in the shape of alphabets such as Y, T and D to realise a birefringence of the order of 10^{-2} as submitted by [6]. Also, the cylindrical symmetry of an ideal fibre can be broken through manipulation of the cladding air holes to obtain high birefringence [7]. These papers have shown photonic crystal structures that achieve birefringence of 10^{-1} to 10^{-4} [5, 8–16]. Also, it has been demonstrated by [17, 18] that the inclusion of elliptical holes in the core can improve birefringence to a very high value of 10^{-2}.

Chromatic dispersion control in optical communication is also critical. If chromatic dispersion is not controlled, it will result in broadening of the optical pulse, which would then cause inter-symbol interference [19]. In PCFs, dispersion consists of waveguide and material. To control chromatic dispersion, the pitch, number of rings of the air holes, the diameter of holes in the cladding, and the number of missing holes can be varied [20]. Dispersion compensation techniques have been investigated by adjusting the hole diameter and hole-to-hole spacing [21, 22]. In [22], rectangular holes were utilised in a core of hexagonal structure to get a birefringence of 10^{-2}. PCF in [23] has been infiltrated by toluene (C_7H_8) to demonstrate that ultra-flattened near-zero dispersion can be achieved.

A square PCF structure with five-air hole rings was utilised in [24] to get an ultra-high birefringence of 4.404×10^{-2}. Another four-ring PCF designed by [25] obtained a 0.6402 ps/nm km chromatic dispersion and 26.27 W^{-1} km^{-1} nonlinearity at 1.3 μm wavelength. Ahmed et al. [24] demonstrated birefringence of 10^{-3} and a zero-dispersion compensation (DC) of 0.9 to 0.95 μm with confinement loss of 39 dB/m for x-polarised mode. Several elliptical PCF structures have been designed by [26–28] to obtain 10^{-2} of birefringence. However these structures and the designs in [17, 18, 25–29] are difficult to fabricate due to the elliptical air holes. A seven-ring square to circular PCF designed by [30] with a high value of birefringence 0.245, a significant negative dispersion of −722.48 ps/km nm and a nonlinear coefficients value of 21.23 ps/km nm at 1.55 μm has been obtained. However, the structure is bulky with several fabrication challenges. A germanium-doped four-ring PCF structure proposed by [31] has reported a low dispersion value of −11.8 ps/km nm with a low nonlinearity of 0.0166 W^{-1} m^{-1} at 1.55 μm, but the work did not report on birefringence. Furthermore, a five-air hole ring [32] with a high nonlinearity value, high birefringence of the order 10^{-2} and very high dispersion of −753 ps/km nm has been suggested. However, this structure is also bulky with some fabrication challenges.

A tuneable zero dispersion was obtained by [33, 34], while [35] reported a large negative, tuneable dispersion by placing seven rectangular air holes inside the core. Despite

these remarkable results, the rectangular holes complicate the fabrication process. High negative dispersion and a birefringence of the order of 10^{-2} has been obtained by [36, 37]. Hassan et al. [38] designed a PCF structure that has demonstrated a high birefringence of 3.15×10^{-2} and two zero dispersion at a range of 0.88–1.20 μm and 1.08–1.29 μm. However, the structure is bulky. Authors in [39] demonstrated that an ultra-flattened dispersion can be obtained in a systematic design of PCF which incorporates odd rings with extra small holes between the lattice. The results also show a nonlinearity value of less than $1.10166 \mathrm{W}^{-1}\,\mathrm{km}^{-1}$.

Research has shown that obtaining high nonlinearity, high birefringence and negative chromatic dispersion is difficult. PCF can be engineered to simultaneously achieve these results. In this paper, step-by-step design has been done with the aim of improving the PCF structure based on the optical properties realised. The optical properties of interest for applications in optical communication, sensing and optical devices are investigated with re-engineering design PCF1 through to PCF4. Hence, the proposed PCF has been obtained from four PCF structures with each tailored towards an optimum structure. This paper demonstrates that it is possible to obtain an ultra-high birefringence of 1.308×10^{-2}, nonlinearity of $30.32 \mathrm{W}^{-1}\,\mathrm{km}^{-1}$ and chromatic dispersion of -24.062 ps/km nm at 1.55 μm with double zero tuneable dispersion at wavelength of 0.99 μm and wavelength of 1.8 μm.

Design methodology

In this work, circular air holes have been used with the air hole rings (Nr) = 4. Silica is used for the background. The refractive index of the silica is described to be wavelength dependent. The Sellmeier equation considered for the structure indicates the relationship between the wavelength and the refractive index which is given by [40] in (1), and the parameters are defined in Table 1. The refractive index is denoted as n, and B_i and C_i represent the Sellmeier coefficients with $n = 1.45$ for pure silica:

$$n^2 = 1 + \frac{B_1\lambda^2}{\lambda^2 - c_1} + \frac{B_2\lambda^2}{\lambda^2 - c_2} + \frac{B_3\lambda^2}{\lambda^2 - c_3} \tag{1}$$

Applying the anisotropic perfectly matched layer (PML) to Maxwell's curl equation, the vectorial equation can be proved in (2):

$$\nabla \times \left(\left[s^{-1}\right]\nabla \times E\right) - k_0^2 n^2[s]E = 0 \tag{2}$$

Table 1 Sellmeier coefficients for pure silica material where $n = 1.45$

Parameters	Values
B1	0.69675
B2	0.408218
B3	0.890815
C1	$4.67914826\mathrm{e}^{-3}$
C2	$1.35120631\mathrm{e}^{-2}$
C3	97.9340025

where E is the electric field vector, $k_0 = 2\pi/\lambda$ is the wave number in vacuum, $[s]^{-1}$ is an inverse matrix of $[s]$, λ is the wavelength, n is the refractive index of the domain, and $[s]$ is the PML matrix.

Chromatic dispersion is considered the combination of waveguide dispersion and material dispersion. Positive values of chromatic dispersion represent an anomalous dispersion, while the negative values of chromatic dispersion represent normal dispersion. The material dispersion hinges on the wavelength dependence on the refractive index of the material which is a result of the interaction between the molecules or electrons in the material, light and ions. The total dispersion of the PCF is computed using (3)

$$D = -\frac{\lambda}{c}\frac{\partial^2 \mathrm{Re}(n_{\mathrm{eff}})}{\partial \lambda^2} \tag{3}$$

where the operating wavelength is denoted by λ. The velocity of light is represented with c, and $R(n_{\mathrm{eff}})$ is the real part of the complex effective index.

Perfectly circular core PCF supports two orthogonal linear polarised modes. These two orthogonal linear polarised modes have the same spatial distribution [41]. These two modes degenerate in an ideal fibre with cylindrical symmetry maintained across its length. Also, the modes degenerate due to the refractive index and associated propagation constants of these modes. These two modes have the same real refractive index values. However, internal stress, deviation in the geometry and bending can cause this symmetry to break, resulting in the two orthogonal linear polarised modes propagating with different velocities. The modal birefringence can be obtained using the equation:

$$B = \left| n_x - n_y \right| \tag{4}$$

where the effective refractive indices are denoted as n_x for x-polarisation, and n_y for y-polarisation fundamental modes, respectively.

If the PCF jacket is considered far from the cladding and the core regions, the guidance of light would be due to the cladding air hole rings which prolong to infinity. Since the layers of the air holes are finite, there is leakage of light from the core to the exterior matrix of the material through the links between the air holes, causing confinement loss [42]. The cladding, made up of finite air holes, causes light to leak from the core towards the exterior, giving rise to confinement loss. Confinement loss can be determined by using the imaginary value of the complex refractive index. Confinement loss (C_{loss}) is calculated by (5)

$$C_{\mathrm{loss}} = \frac{40\pi}{\ln(10)\lambda}\mathrm{Im}(n_{\mathrm{eff}})\left[\frac{\mathrm{dB}}{\mathrm{m}}\right] \tag{5}$$

The imaginary part of the effective refractive index is denoted as I_{m} (n_{eff}).

Effective mode area is determined by computing the integral transformation to the ends and face of the whole fibre. The effective mode area is given by equation in (6), where E gives the amplitude of the transverse electric field.

$$A_{\mathrm{eff}} = \frac{\left(\iint |E|^2 \mathrm{d}x\mathrm{d}y\right)^2}{\iint |E|^4 \mathrm{d}x\mathrm{d}y} \tag{6}$$

Nonlinear optical effects are noticed when the power density of the light is large enough, no matter the type of material used. The nonlinear coefficient is a parameter that is inversely proportional to the effective mode area [43] and given by Eq. (7);

$$\gamma = \frac{2\pi}{\lambda}\frac{n_2}{A_{\text{eff}}} \tag{7}$$

where the nonlinear refractive index coefficient of the material is denoted n_2 which in this work relates to 2.76×10^{-20} m^2/W.

Design and method for proposed structure

A hexagonal structure with circular air hole cladding and a solid core is presented. The optimised design starts with PCF1, which has the lattice, Λ, of the cladding region at 2.3 μm. This structure is designed with an air filling fraction of 0.6. The holes in the rings have been drawn with an air hole size of diameters: $d_1 = 1.5d$, $d_2 = 1.25d$, $d_3 = d$ and $d_4 = 0.75d$, respectively, as shown in Fig. 1a, where diameter $d = 1.38$ μm. It is well known that a large index contrast cannot be obtained in conventional fibres. In PCF however, significant refractive index contrast can be realised with large holes in the cladding, which give rise to a very high birefringence and large chromatic dispersion.

On the other hand, a small refractive index contrast between the cladding and the core can be realised by using small air holes in the cladding, reducing birefringence. A descending air hole ring is used for this work to realise a refractive index contrast that would achieve a very low confinement loss and low effective mode area. Figure 1b shows the fundamental mode profile of x-polarisation at the wavelength of 1.55 μm, indicating very high light confinement in the core. The other three PCFs have been designed to help improve the properties of interest. All four PCFs have been surrounded by PML of regions 1–3 with the computational domain in the direction x and y, marked as W_x and W_y, respectively. The parameters $W = 2$ μm, $W_x = 20.6$ μm and $W_y = 24$ μm, and the refractive index of air is 1.0. Propagation in the Z direction is assumed throughout the analysis.

The design is continued as shown in Fig. 2a (PCF2), which has the lattice, Λ, of the cladding region at 1.7 μm. This structure is designed with an air filling fraction of 0.6. The holes in the rings have been drawn with air hole size of diameters: $d_1 = 1.5d$, $d_2 = 1.25d$, $d_3 = d$ and $d_4 = 0.75d$ respectively, where diameter, $d = 1.02$ μm. The PCF2 has been designed to improve the birefringence in PCF1. To accomplish this, the holes at orthogonal axes between rings one and two were changed to have an air filling fraction of $d_4/\Lambda = 0.45$ and $d_5/\Lambda = 0.55$ as shown in Fig. 2a. In Fig. 2b (i), (ii), (iii) and (iv) are profiles of the fundamental mode at the wavelength of 1.55 μm for x and y-polarisation modes which indicates high light confinement in the core.

Further to the PCF2 structure, PCF3 is designed with tiny holes introduced between the holes at the orthogonal axes (rings 1 and 2) to improve birefringence further and decrease the value of the confinement loss. The tiny holes of air filling fraction; $d_4/\Lambda = 0.22$ and $d_6/\Lambda = 0.9$ have been introduced into the holes in the middle of the first and second ring to improve the dispersion. The structure of PCF3 is illustrated in Fig. 3a. The rest of the air holes have been maintained as indicated in PCF2. The fundamental

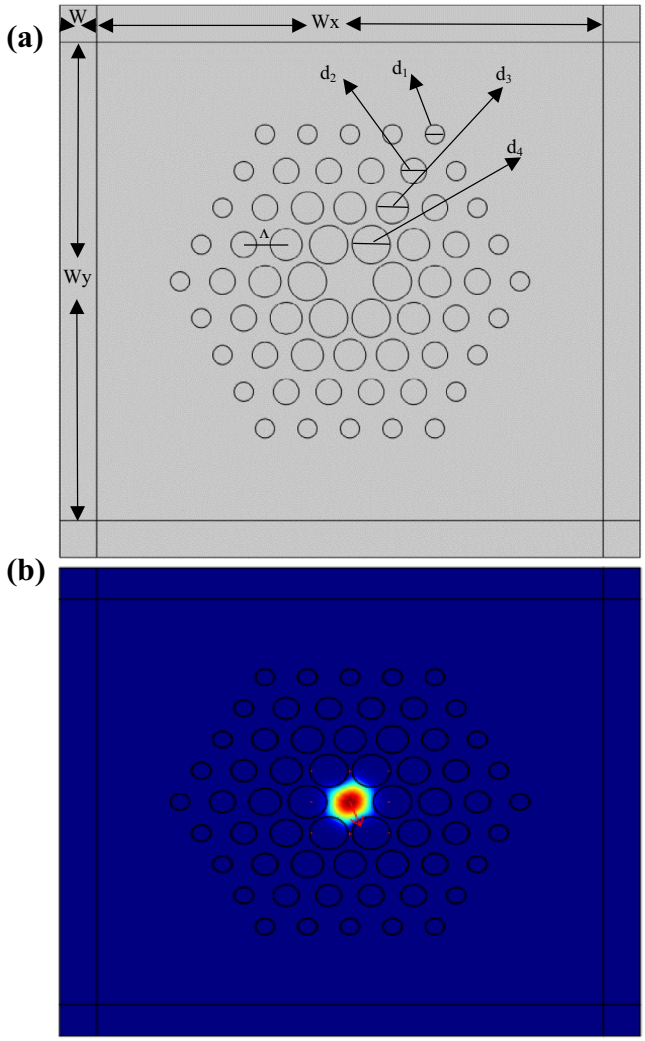

Fig. 1 **a** The cross-section of the descending hole arrangement, PCF1. **b** Fundamental mode profile at 1.55 μm of *x*-polarisation mode PCF1

mode profile of the PFC3 at *x*- and *y*-polarisation for wavelength at 1.55 μm is shown in Fig. 3b, c, respectively.

The final design, shown in Fig. 4a (PCF4), is the optimised PCF structure obtained from PCF1 through to PCF3. The tiny holes introduced in PCF3 between the first and second ring of the orthogonal axes have been removed to study the dispersion further, even though the birefringence is very high. The fundamental mode profiles of *x*- and *y*-polarisation modes at 1.55 μm are represented in Fig. 4b, c.

Results and analysis

Analysis of PCF1

The chromatic dispersion investigated relates to the real part of the complex effective index. In Fig. 5, which refers to PCF1, it can be observed that the effective index values decreases with an increase in the values of the wavelength. At 1.55 μm, the real

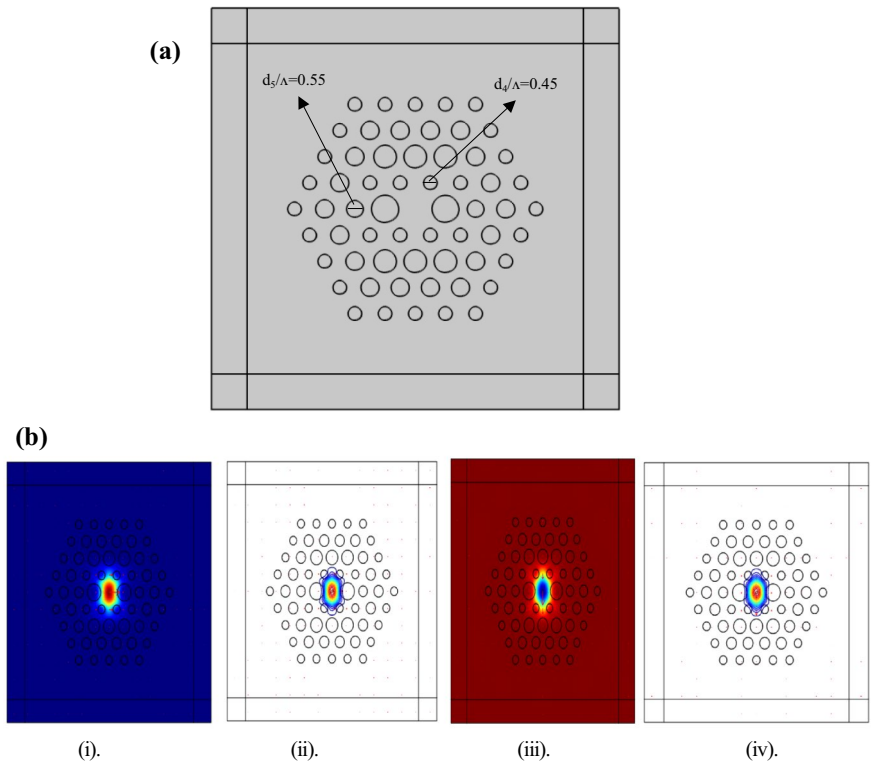

Fig. 2 **a** Cross-section of the PCF2 structure. **b** The fundamental mode profiles at 1.55 µm for *X*-polarisation (i, ii). *Y*-polarisation (iii, iv)

effective index of 1.3928 µm for both *x*- and *y*-polarisation is obtained. It can be seen from Fig. 5 that there is no difference in the *x*- and *y*-polarisation modes, indicating that the birefringence is very low or insignificant. The descending air hole arrangement gives a very low birefringence at a pitch of 2.3 µm.

C_{loss} of the fundamental mode is calculated using the imaginary part of the complex effective index. C_{loss} for PCF1 is very low, as seen in the mode profile Fig. 1b, which shows the high confinement of light inside the core. A low C_{loss} of $7.48843937 \times 10^{-6}$ dB/m and $1.53051855 \times 10^{-5}$ dB/m for *x*- and *y*-polarised modes at 1.55 µm have been achieved. The descending air hole arrangement demonstrates very low C_{loss}, as shown in Fig. 6.

Figure 7 depicts the effect of the descending hole arrangement on the effective mode area. The effective mode area grows as the wavelength gets longer. PCF1's effective mode area at 1.55 µm is $3.83 \times 10\ \text{m}^2$, showing a small effective mode area.

The chromatic dispersion of PCF1 is depicted in Fig. 8. At 1.55 µm, the chromatic dispersion value is 175 ps/km nm. This indicates that chromatic dispersion is positive for all wavelengths between 1.0 and 1.8 µm.

(See figure on next page.)

Fig. 3 **a** Cross-section of the structure of PCF3. **b** The field profile of the fundamental mode at the wavelength of 1.55 µm for *X*-polarisation mode. **c** The field profile of the fundamental mode at the wavelength of 1.55 µm for *Y*-polarisation mode

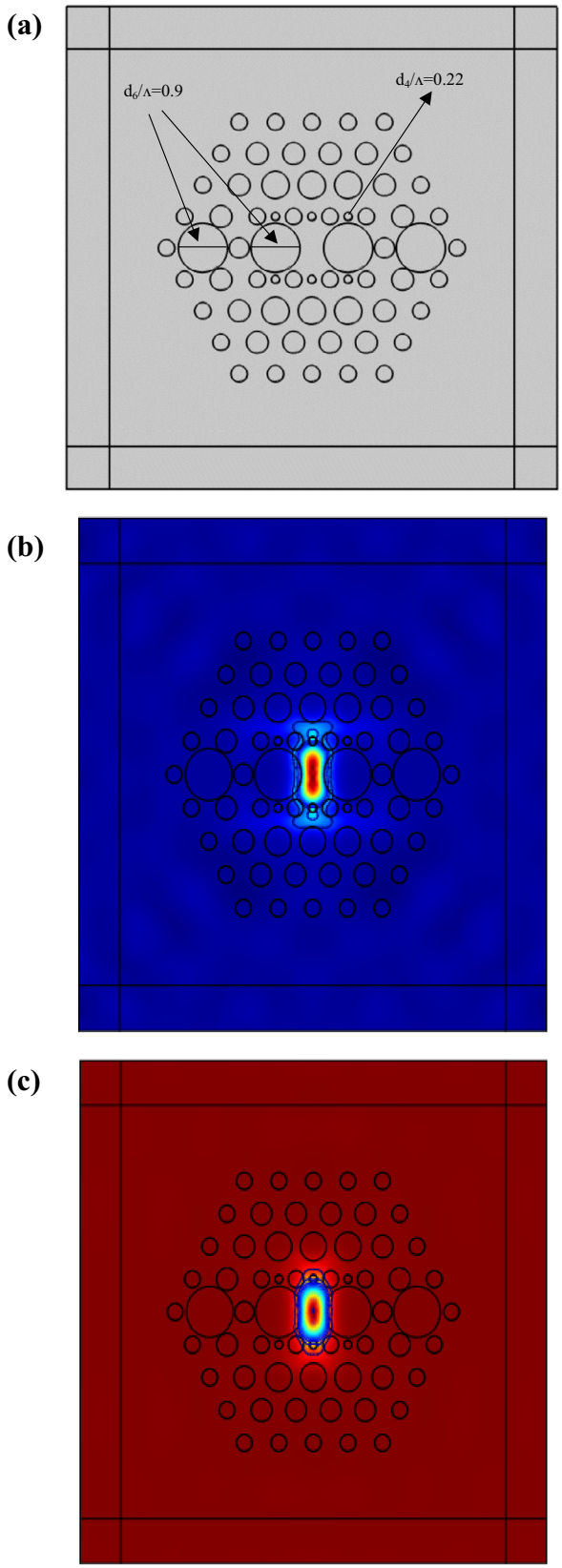

Fig. 3 (See legend on previous page.)

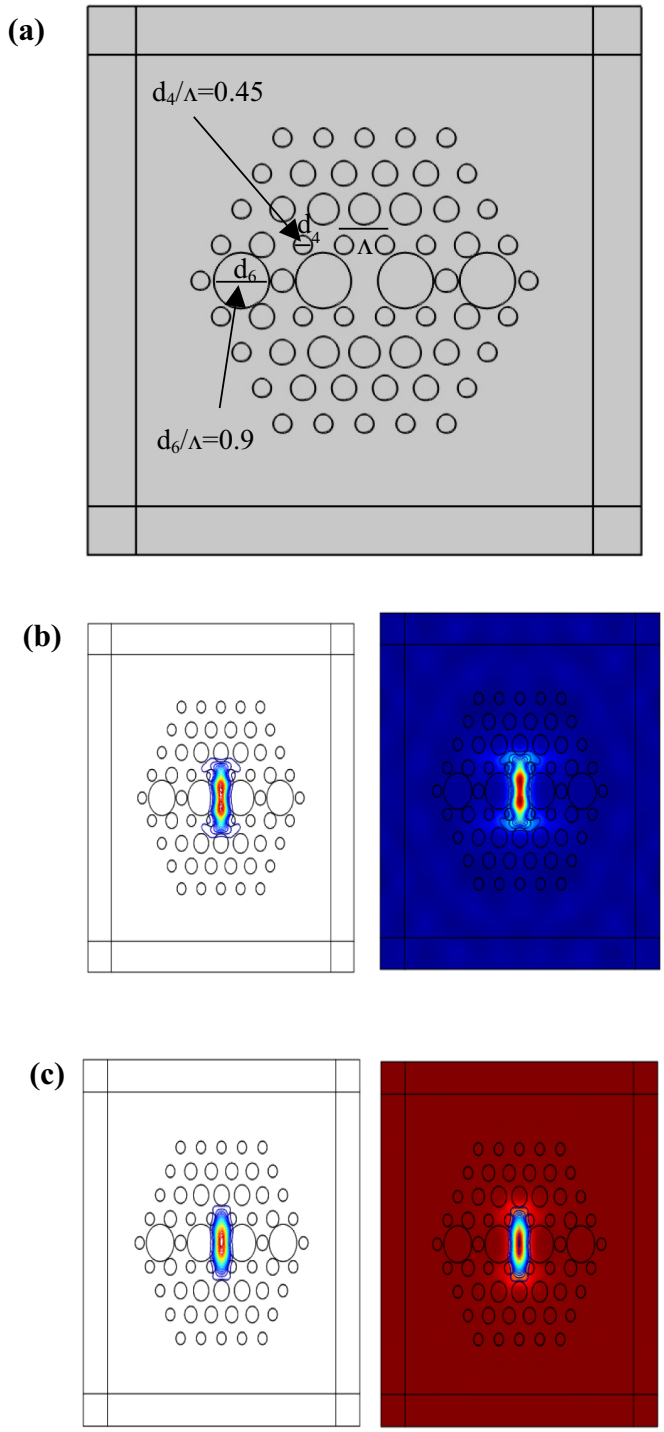

Fig. 4 **a** Cross-section of PCF4. **b** Fundamental mode profile at the wavelength of 1.55 μm for *X*-polarisation mode. **c** Fundamental mode profile at the wavelength of 1.55 μm for *Y*-polarisation mode

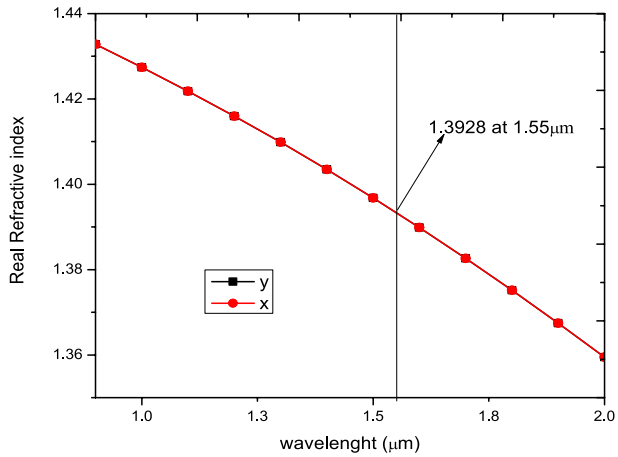

Fig. 5 Real effective index as a function of wavelength Λ = 2.3 μm for PCF1

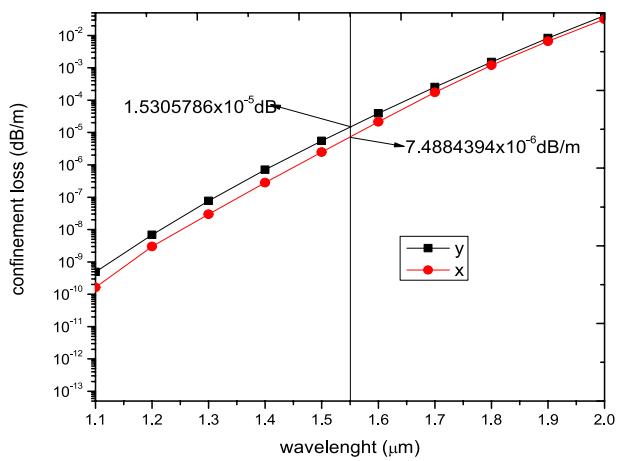

Fig. 6 C_{loss} as a function of wavelength Λ = 2.3 μm for PCF1

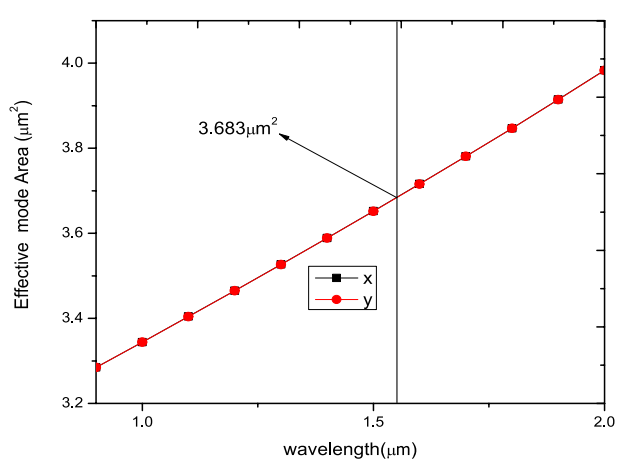

Fig. 7 Effective mode area as a function of wavelength Λ = 2.3 μm for PCF1

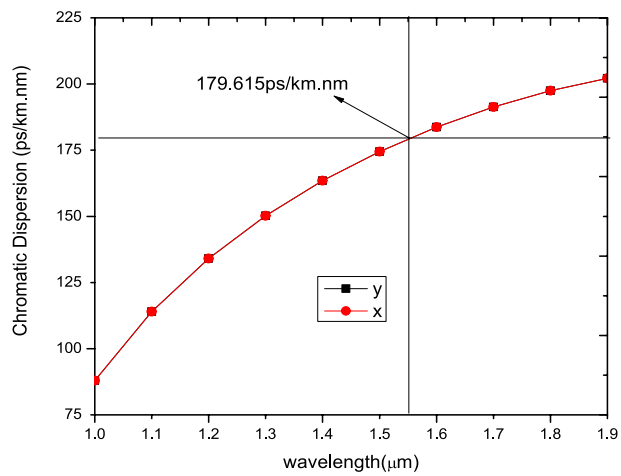

Fig. 8 Chromatic dispersion as a function of wavelength, Λ = 2.3 μm for PCF1

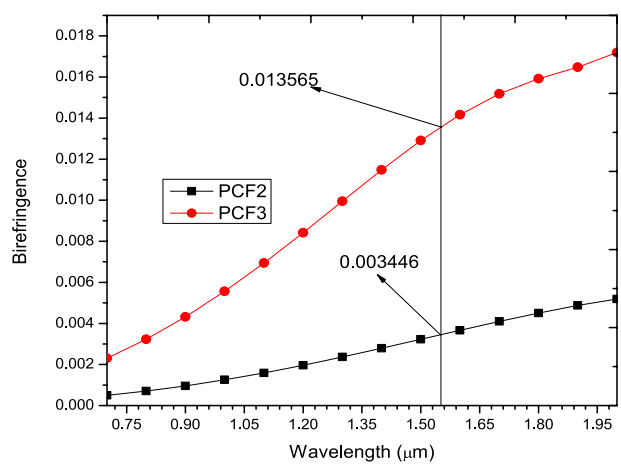

Fig. 9 Variation of Birefringence as a function of wavelength for PCF2 and PCF3

Analysis for PCF2 and PCF3

Birefringence performance analysis of PCF2 and PCF3

Figure 9 demonstrates the link between birefringence and wavelength for PCF2 and PCF3. In PCF2, the birefringence of 10^{-3} is recorded at all the wavelengths, but for PCF3, 10^{-3} is realised only at shorter wavelengths and 10^{-2} for longer wavelengths. The influence of the change of hole sizes on the orthogonal axes has yielded an improvement. Also, the results show that changing the air filling fraction $d_4/\Lambda = 0.45$ and $d_6/\Lambda = 0.55$ has increased the birefringence significantly. In PCF3, holes with air filling fractions $d_4/\Lambda = 0.22$ and $d_5/\Lambda = 0.9$ have been introduced, causing the birefringence to increase further. The birefringence at 1.55 μm is 0.003446 for PCF2 and 0.013565 for PCF3. This means the value of birefringence increased from 10^{-3} to 10^{-2}, which is better than [44]. The birefringence of PCF3 is in agreement with [45], while that of PCF2 is in agreement with [46].

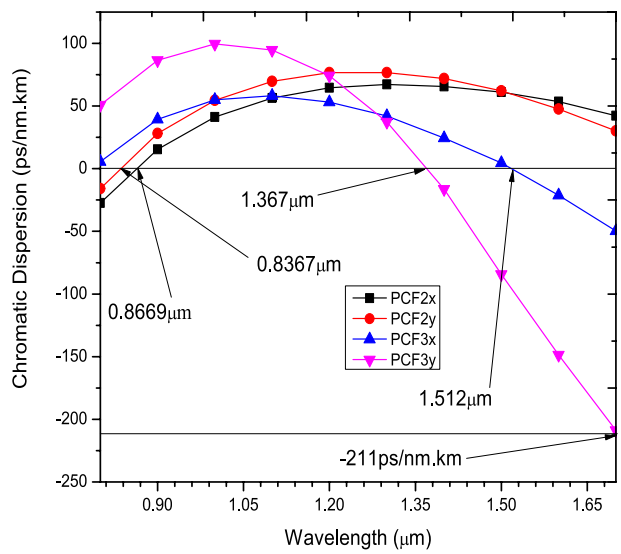

Fig. 10 Change of Chromatic dispersion as a function of wavelength for PCF2 and PCF3

Chromatic dispersion for PCF2 and PCF3

Figure 10 shows chromatic dispersion for both PCF2 and PCF3. The modal fields are confined to the silica at shorter wavelengths, whereas the effective cladding index falls at longer wavelengths. The zero chromatic dispersion (ZD) changes as the diameter of the air hole and the pitch change. The graph also shows how changing the geometrical parameters can shift the zero-dispersion wavelength from visible to infrared regions. According to the results, zero-dispersion wavelength is realised for x- and y-polarisation of PCF2 at 0.8669 μm and 0.8367 μm, respectively. In the x- and y-polarisation modes, PCF3 registers zero-dispersion at wavelengths of 1.512 μm and 1.367 μm, respectively. These demonstrate a double tuneable zero dispersion. A very high negative dispersion of −211 ps/nm km can be observed at a wavelength of 1.7 μm for PCF3 at y-polarisation mode. Also, the chromatic dispersion for the PCF2 is higher than that of PCF3 at 1.55 μm. The chromatic dispersion at 1.55 μm for PCF3 is −9.55 ps/nm km. Therefore, the air hole d_5 has reduced dispersion along longer wavelengths.

Confinement loss for PCF2 and PCF3

C_{loss} is determined by the imaginary part of the complex effective index. The performance of the confinement loss is demonstrated in Fig. 11. The analysis of confinement loss on the PCF2 and PCF3 as regards the change of $d_4/\Lambda = 0.45$ and $d_6/\Lambda = 0.55$ in PCF2 to $d_4/\Lambda = 0.22$ and $d_6/\Lambda = 0.9$ in PCF3 is indicated in Fig. 11. At a wavelength of 1.55 μm, PCF2 performed better than PCF3. At a wavelength of 1.55 μm, PCF3 achieved a C_{loss} of 33.65 dB/m. However, the air holes with $d_4/\Lambda = 0.45$ and $d_6/\Lambda = 0.55$ reduced the confinement loss to 0.2631 dB/m. This shows that the air with $d_4/\Lambda = 0.45$ introduced into the first ring at the orthogonal axes and the air hole ring with $d_6/\Lambda = 0.55$ introduced into the second ring at the centre demonstrate low

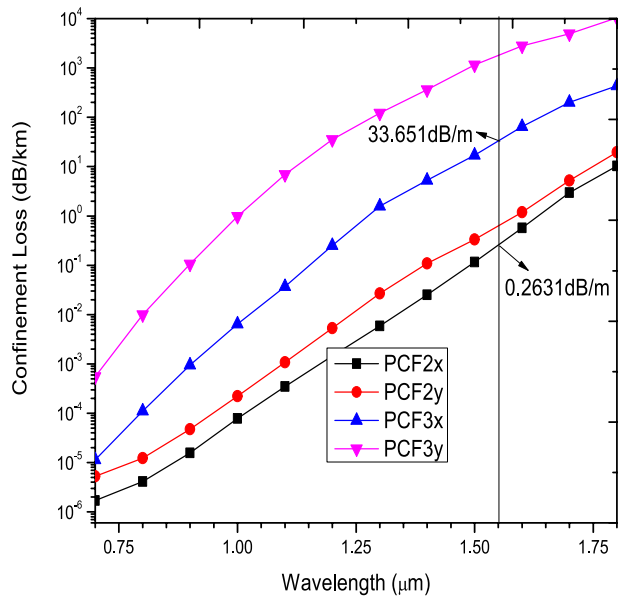

Fig. 11 Variation of confinement loss as a function of wavelength for PCF2 and PCF3

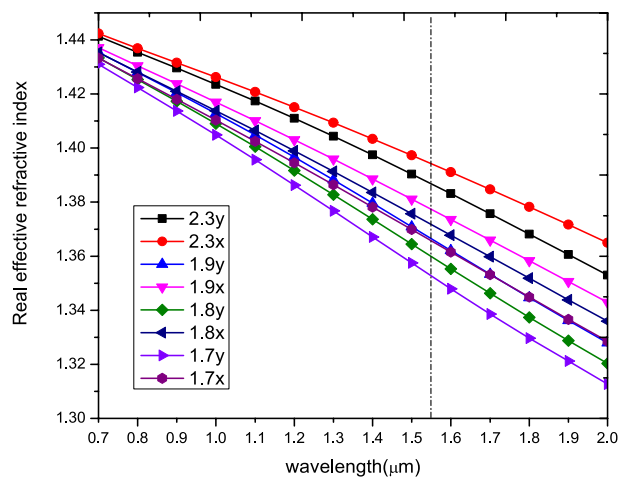

Fig. 12 Change of real effective index as a function of wavelength Λ of 1.7 μm, 1.8 μm, 1.9 μm and 2.3 μm

confinement loss. The performance of PCF2 and PCF3, as seen in Fig. 11, shows that as the wavelength increases, the confinement loss also increases.

Analysis of PCF4

PCF4 is the optimised structure from PCF1 to PCF3. The real effective index, the Birefringence, Effective mode area, $C_{\text{loss,}}$ nonlinearity, and chromatic dispersion for PCF4 are discussed in this section. The pitch is varied from 1.7 to 2.3 μm to analyse the effect of change in Pitch with respect to the wavelength on the optical properties. In addition, the effect of the change in pitch on the real part of the effective index is analysed in this section.

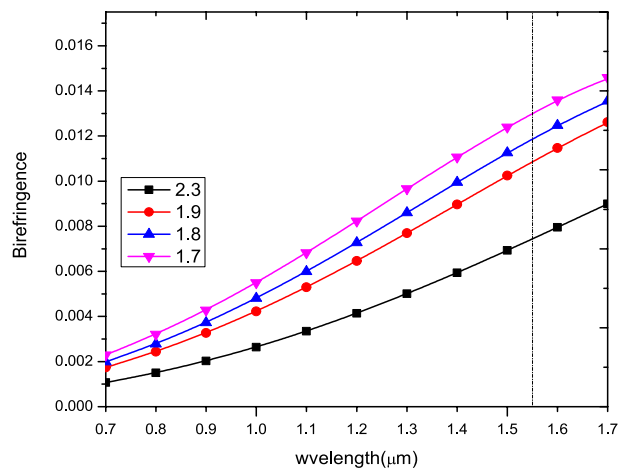

Fig. 13 Change of Birefringence as a function of wavelength Λ of 1.7 μm, 1.8 μm, 1.9 μm and 2.3 μm for PCF4

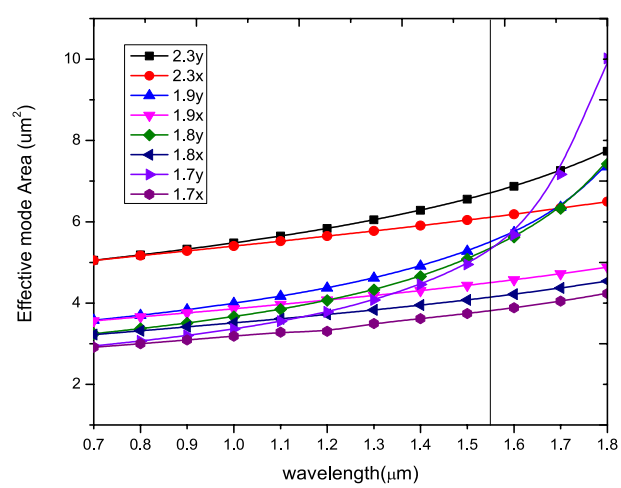

Fig. 14 Change of effective mode area as a function of wavelength for Λ of 1.7 μm, 1.8 μm, 1.9 μm and 2.3 μm

Real effective index and birefringence for PCF4

The results obtained for the performance of PCF4 in terms of the real portion of the effective refractive index in Fig. 12 shows that refractive index decreases monolithically with respect to increase in the operating wavelength. The graph also indicates that the real effective index increases as hole-to-hole spacing increases.

In Fig. 13, the results show an ultra-high birefringence of the order of 10^{-2} at 1.55 μm for a hole-to-hole spacing of 1.7 μm, 1.8 μm and 1.9 μm, which agrees with [17, 19, 24, 27, 37, 38] and better than [15, 47, 48]. Also, Fig. 13 indicates birefringence of 10^{-2}, which is maintained over the O to U optical communication band for the hole-to-hole spacing of 1.7 μm, 1.8 μm and 1.9 μm. The Birefringence for PCF3 is in the same range as PCF4. The Birefringence value decreased at the pitch 2.3 μm from 10^{-2} to 10^{-3}.

Effective mode area and nonlinearity for PCF4

Nonlinearity is not examined in PCF1, PCF2 and PCF3 because the focus is to examine the performance of birefringence, C_{loss}, and chromatic dispersion as the key optical parameters. Following a significant improvement in birefringence in PCF3 and PCF4, the work is broadened to include effective mode area and nonlinearity to determine the performance of the optimum PCF4 structure. Figure 14 shows the effective mode area as a function of wavelength, indicating that the effective mode area increases as the operating wavelength increases. The reason is that, as the wavelength increases, the mode leaks through the air holes. A nonlinear coefficient of 30.32 w^{-1} km^{-1} is obtained for the hole-to-hole spacing of 1.7 μm. The effective mode area that is used to calculate the nonlinearity is shown in Fig. 15. The nonlinearity decreases with an increase in the operating wavelength. The nonlinearity for PCF4 with pitch value of 1.7 μm is 30.32 w^{-1} km^{-1} better than [25] and close to [37, 38].

Chromatic dispersion and confinement loss for PCF4

Figure 16 indicates the chromatic dispersion, which increases at the shorter wavelength from negative steadily, crossing the zero line for all the values of $\Lambda = 1.7$ μm, 1.8 μm, 1.9 μm and 2.3 μm. The graph indicates a double negative chromatic dispersion for all the hole-to-hole spacing from −263.87 to −2.6845 ps/km nm and from −22.907 to −234.055 ps/km nm at wavelength ranges of 0.8–0.9 μm and 1.5–1.8 μm, respectively. Also, double zero dispersion is realised at the pitches of 1.7 μm and 1.8 μm.

In Fig. 17, the value of the confinement loss is 37 dB/m at 1.55 μm for a pitch of 1.7 μm. Figure 17 also shows that confinement loss increases as the hole-to-hole spacing at the cladding decreases [49]. The confinement loss at hole-to-hole spacing of 2.3 μm is 0.200725 dB/m at *x*-polarisation mode, which is better than PCF2 and PCF3.

Hole pitch as a function of real effective index

The effect of pitch on the real part of the complex effective index can be observed in Fig. 18. The results indicate that the hole-to-hole spacing (Λ) increases with an increase

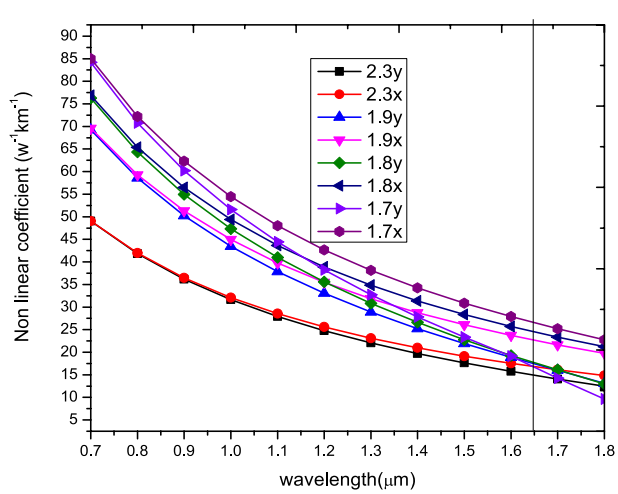

Fig. 15 Change of nonlinear coefficient as a function of wavelength Λ of 1.7 μm, 1.8 μm, 1.9 μm and 2.3 μm for PCF4

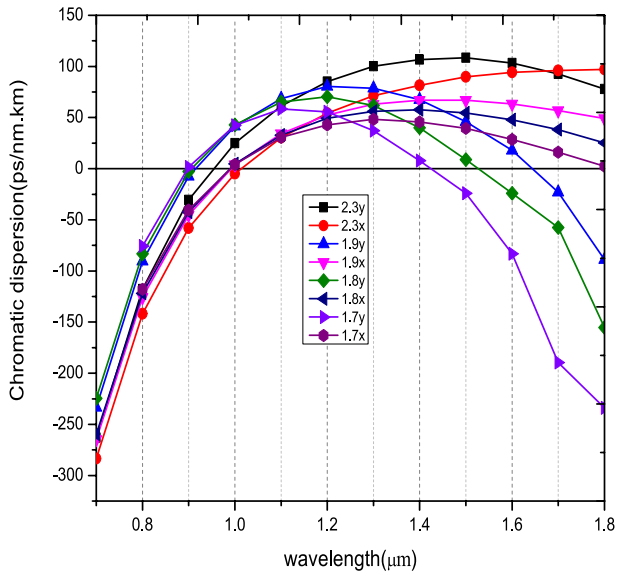

Fig. 16 Change of chromatic dispersion as a function of wavelength at the pitch; 1.7 μm, 1.8 μm, 1.9 μm, and 2.3 μm

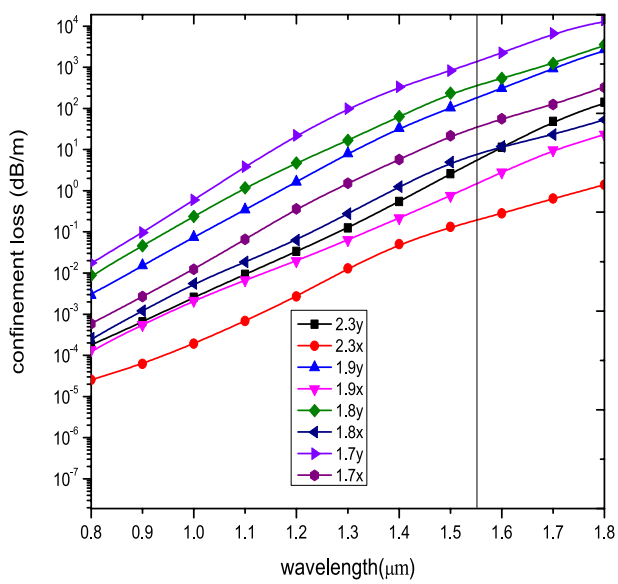

Fig. 17 Change of confinement loss as a function of wavelength at pitch 1.7 μm, 1.8 μm, 1.9 μm and 2.3 μm for PCF4

in the real effective index. This demonstrates that the hole sizes at the core affect the effective index.

Table 2 compares the performance of the proposed design PCF4 results against other related works.

PCFs are made in a variety of ways, including stack and draw, mechanical drilling [8], Sol–gel [50, 51] and extrusion [52]. The traditional stack and draw approach is appropriate for fabricating the proposed PCF structure because the circular air hole and triangular lattice make manufacturing simple and precise [53]. Mechanical drilling can also be

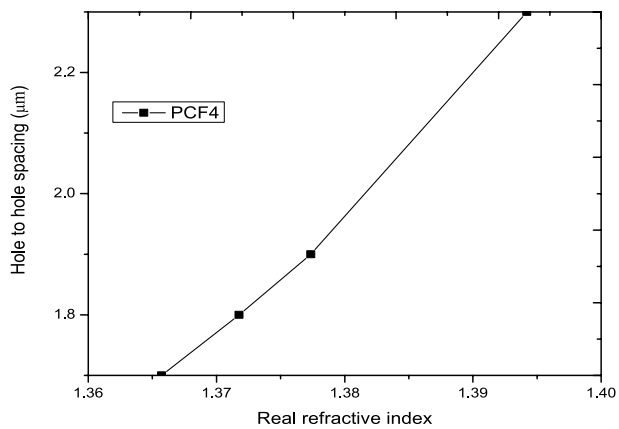

Fig. 18 Variation of pitch as a function of real part of the effective index for *x*-polarisation mode

Table 2 Evaluation of the proposed PCF with other published designs

Study references	Confinement loss (dB/m) at 1.55 μm	Wavelength at ZD μm	Birefringence at 1.55 μm	Nonlinearity at 1.55 μm	Ring
[29]	$X=190.28$ $y=39.22$	0.9, 0.95	6.93×10^{-3}	–	2-circular holes and 3 elliptical holes
[38]	$X=89.4, y=17.6$	$X=1.08, 1.29$ $Y=0.88, 1.20$	3.15×10^{-2}	58 w^{-1} km^{-1}	6-circular holes
[9]	–	–	8×10^{-3}	–	6-elliptical and rhombic holes
[8]		1.87	9.23×10^{-3}	–	9- circular holes
[25]	–	–	–	At 1.33 μm = 26.7 w^{-1} km^{-1}	4-circular holes
[32]	–	–	3.87×10^{-2}	96.51 w^{-1} km^{-1}	5-circular holes
[30]	0.11	–	2.45×10^{-1}	21.23 w^{-1} km^{-1}	7-square to circular holes
[31]	–	–	–	0.0166w^{-1} m^{-1}	4-circular holes
Proposed PCF Fig. 4a					4-all circular holes
$\Lambda=1.7$ μm	$X=3.76\times10^{1}$ $Y=1.34\times10^{3}$	$x=0.99, 1.8$ $y=0.90, 1.42$	1.308×10^{-2}	$X=30.32$ $Y=21.90$	
$\Lambda=1.8$ μm	X = 8.53 Y = 3.77	$x=0.99$ $y=0.90, 1.52$	1.188×10^{-2}	$X=27.89$ $Y=21.66$	
$\Lambda=1.9$ μm	$X=1.55$ $Y=1.85\times10^{2}$	$x=0.99$ $y=0.90, 1.64$	1.086×10^{-2}	$X=25.64$ $Y=21.05$	
$\Lambda=2.3$	$X=0.20075$ $Y=5.584$	$x=1$ $y=0.95$	7.0×10^{-3}	$X=18.95$ $Y=17.23$	

employed to make the suggested PCF because the hole sizes and spacing can be changed [50]. PCFs with triangular lattice structures have been made using the stack and draw technique [54–58], indicating that the proposed structure can be fabricated.

Conclusion

Optical fibre structures suffer from the dispersion of signals leading to inter-symbol interference; hence, a zero chromatic dispersion at a specified wavelength is desirable. An ultra-high Birefringence is a property that is essential in sensing applications. In

this paper, multiple optical properties of fibre structure are obtained. A single design presented in some works to demonstrate some optical properties does not show how the various placement of holes influences the optical properties and how the final structure is optimised. The proposed PCF is a step-by-step design approach. Four structures have been considered and configured. The results show a nonlinear coefficient of 30.32 w^{-1} km^{-1}, a negative chromatic dispersion of -24.062 ps/km nm and ultra-high Birefringence of 1.308×10^{-2} at 1.55 μm with double zero tuneable dispersion at wavelengths of 0.9 μm and 1.8 μm for x-polarisation and 0.99 μm and 1.42 μm for y-polarisation. The proposed PCF is suitable for high-speed communication systems, optical communication, optical devices and sensing. This proposed PCF structure with circular air holes can be fabricated using the stack and draw method.

Acknowledgements
Not applicable.

Author contributions
PAA carried designed of the structures, did coordination and drafted the manuscript. AKA participated in editing of the manuscript. EKA participated in the analysis and final review. All authors read and approved the final manuscript.

Funding
This research did not receive any specific grant from funding agencies in the public, commercial, or not-for-profit sectors.

Availability of data and materials
All material and data have been included in the manuscript.

Declarations

Competing interests
The authors declare that they have no competing interests.

Received: 26 April 2022 Accepted: 13 April 2023
Published online: 25 April 2023

References

1. Kurokawa K et al (2006) Penalty-free dispersion-managed soliton transmission over a 100-km low-loss PCF. J Lightwave Technol 24(1):32
2. Thévenaz L (2011) Advanced fiber optics. EPFL Press
3. Lee YS, Hong S, Kim SE, Oh K (2018) Dense double-cladding photonic crystal fiber with high birefringence, large negative dispersion and high nonlinearity. In: 2018 23rd Opto-electronics and communications conference (OECC), pp 1–2. IEEE
4. Ghunawat AK, Chandra R, Singh G (2017) Design of an ultra-flattened negative dispersion elliptical spiral photonic crystal fiber with high nonlinearity and high birefringence. In: 2017 International conference on computer, communications and electronics (Comptelix), pp 623–627. IEEE
5. Hasan MR, Islam MA, Rifat AA, Hasan MI (2017) A single-mode highly birefringent dispersion-compensating photonic crystal fiber using hybrid cladding. J Mod Opt 64(3):218–225
6. Gautam A, Mahato D, Kumar P (2018) Design of photonic crystal fibers for high data rate transfer at ultra low confinement loss. In: 2018 International conference on communication and signal processing (ICCSP), pp 0354–0357. IEEE
7. Ortigosa-Blanch A et al (2000) Highly birefringent photonic crystal fibers. Opt Lett 25(18):1325–1327
8. Lee YS, Lee CG, Bahloul F, Kim S, Oh K (2019) Simultaneously achieving a large negative dispersion and a high birefringence over Er and Tm dual gain bands in a square lattice photonic crystal fiber. J Lightwave Technol 37(4):1254–1263
9. Gao Y et al (2019) Highly-birefringent and ultra-wideband low-loss photonic crystal fiber with rhombic and elliptical holes. Opt Commun
10. Islam MI et al (2019) Proposed square lattice photonic crystal fiber for extremely high nonlinearity, birefringence and ultra-high negative dispersion compensation. J Opt Commun 40(4):401–410
11. Yang T, Ding C, Ziolkowski RW, Guo YJ (2018) High birefringent ENZ photonic crystal fibers. In: 2018 International conference on numerical simulation of optoelectronic devices (NUSOD), pp 85–86. IEEE
12. Ademgil H, Haxha S (2015) PCF based sensor with high sensitivity, high birefringence and low confinement losses for liquid analyte sensing applications. Sensors 15(12):31833–31842
13. Ademgil H, Haxha S (2016) Highly birefringent nonlinear PCF for optical sensing of analytes in aqueous solutions. Optik 127(16):6653–6660

14. Arif MFH, Biddut MJH (2017) Enhancement of relative sensitivity of photonic crystal fiber with high birefringence and low confinement loss. Optik 131:697–704
15. Yang T-J, Shen L-F, Chau Y-F, Sung M-J, Chen D, Tsai DP (2008) High birefringence and low loss circular air-holes photonic crystal fiber using complex unit cells in cladding. Opt Commun 281(17):4334–4338
16. Arhinful F, Akowuah EK, Danlard I, Dede A (2022) A highly birefringent negative chromatic dispersion photonic crystal fibre for long-haul transmission: design and analysis. Results Opt 9:100325
17. Halder A, Hossain SA (2016) Design of ultra-high birefringent broadband dispersion compensating photonic crystal fiber for high speed transmission system. Imperial J of Interdisc Res 2:211
18. Liu Q et al (2019) A high-birefringent photonic quasi-crystal fiber with two elliptical air holes. Optik
19. Lee YS, Lee CG, Jung Y, Oh M-K, Kim S (2016) Highly birefringent and dispersion compensating photonic crystal fiber based on double line defect core. J Opt Soc Korea 20(5):567–574
20. Arif MFH, Biddut MJH (2017) A new structure of photonic crystal fiber with high sensitivity, high nonlinearity, high birefringence and low confinement loss for liquid analyte sensing applications. Sens Bio-Sens Res 12:8–14
21. Kahlon N, Kaur G (2014) Various dispersion compensation techniques for optical system: a survey. Open J Commun Softw 1(1):64–73
22. Ni Y, Zheng X, Ma R (2016) Broadband dispersion compensation technology in high speed optical fiber communication systems
23. Thi TN, Trong DH, Van LC (2023) Supercontinuum generation in ultra-flattened near-zero dispersion PCF with C7H8 infiltration. Opt Quant Electron 55(1):1–22
24. Ahmed F, Kumar P, Hakim MA, Miah MS, Al Noman A, Biswas SK (2018) Ultrahigh birefringence and highly nonlinear square photonic crystal fiber for S+ C+ L+ U wavebands. In: 2018 9th International conference on computing, communication and networking technologies (ICCCNT), pp 1–4. IEEE
25. Chauhan P, Kumar A, Kalra Y (2019) A dispersion engineered silica-based photonic crystal fiber for supercontinuum generation in near-infrared wavelength region. Optik 187:230–237
26. Hasanuzzaman G, Rana S, Habib MS (2016) A novel low loss, highly birefringent photonic crystal fiber in THz regime. IEEE Photonics Technol Lett 28(8):899–902
27. Saha R, Hossain MM, Rahaman ME, Mondal HS (2019) Design and analysis of high birefringence and nonlinearity with small confinement loss photonic crystal fiber. Front Optoelectron 12:165–173
28. Sonne A, Ouchar A (2015) Improving of high birefringence photonic crystal fiber with low confinement loss using small elliptical air holes in the core region. J Mod Opt 62(7):588–592
29. Gangwar RK, Singh VK (2016) Study of highly birefringence dispersion shifted photonic crystal fiber with asymmetrical cladding. Optik 127(24):11854–11859
30. Prajapati YK, Kumar R, Singh V (2019) Design of a photonic crystal fiber for dispersion compensation and sensing applications using modified air holes of the cladding. Braz J Phys 49(5):745–751
31. Prajapati Y, Srivastava V, Singh V, Saini J (2018) Effect of germanium doping on the performance of silica based photonic crystal fiber. Optik 155:149–156
32. Biswas SK, Islam S, Islam M, Mia MMA, Sayem S, Ahmed F (2018) Design of an ultrahigh birefringence photonic crystal fiber with large nonlinearity using all circular air holes for a fiber-optic transmission system. Photonics 5(3):26
33. Yu C-P, Liou J-H, Huang S-S, Chang H-C (2008) Tunable dual-core liquid-filled photonic crystal fibers for dispersion compensation. Opt Express 16(7):4443–4451
34. Yang T, Ding C, Guo YJ (2018) A highly birefringent and nonlinear $AsSe_2$–As_2S_5 photonic crystal fiber with two zero-dispersion wavelengths. IEEE Photonics J 11(1):1–7
35. Huang D, Huang Z, Zhan D (2018) Novel large negative dispersion and tunable zero dispersion wavelength of photonic crystal fiber. Waves Random Complex Media 28(4):624–629
36. Biswas SK et al (2019) A modified design of a hexagonal circular photonic crystal fiber with large negative dispersion properties and ultrahigh birefringence for optical broadband communication. Photonics 6(1):19
37. Tabassum N, Rashid MM, Yesmin A, Islam ME (2019) Highly nonlinear and highly birefringent hybrid photonic crystal fiber. In: 2019 International conference on robotics, electrical and signal processing techniques (ICREST), pp 292–296. IEEE
38. Hasan MR, Anower MS, Hasan MI (2016) Polarization maintaining highly nonlinear photonic crystal fiber with closely lying two zero dispersion wavelengths. Opt Eng 55(5):056107
39. Huang Y, Yang H, Mao Y (2021) Design of linear photonic crystal fiber with all-positive/negative ultraflattened chromatic dispersion for the whole telecom band. Opt Eng 60(7):076110
40. Bjarklev A, Broeng J, Bjarklev AS (2012) Photonic crystal fibres. Springer
41. Zolla F (2005) Foundations of photonic crystal fibres. Imperial College Press
42. White T, McPhedran R, de Sterke CM, Botten L, Steel M (2001) Confinement losses in microstructured optical fibers. Opt Lett 26(21):1660–1662
43. Agrawal GP (2000) Nonlinear fiber optics. In: Nonlinear science at the dawn of the 21st century. Springer, pp 195–211
44. Faisal M, Bala A, Roy Chowdhury K, Mia MB (2018) Highly birefringent large negative dispersion-flattened photonic crystal fibre for broadband residual dispersion compensation. J Mod Opt 65(13):1577–1583
45. Paul BK, Ahmed K (2019) Highly birefringent TOPAS based single mode photonic crystal fiber with ultra-low material loss for Terahertz applications. Opt Fiber Technol 53:102031
46. Ahmed K et al (2018) Ultra high birefringence and lower beat length for square shape PCF: analysis effect on rotation angle and eccentricity. Alex Eng J 57(4):3683–3691
47. Olyaee S, Taghipour F (2011) Design of new square-lattice photonic crystal fibers for optical communication applications. Int J Phys Sci 6(18):4405–4411
48. Kim J (2023) High birefringence and near-zero dispersion control of nonlinear photonic crystal fibers with a double-cladded coaxial core. Microw Opt Technol Lett
49. Akowuah E, Ademgil H, Haxha S (2012) Design and analysis of photonic crystal fibres (PCFs) for broadband applications. In: 2012 IEEE 4th international conference on adaptive science & technology (ICAST), pp 114–120. IEEE

50. Bise RT, Trevor DJ (2005) Sol–gel derived microstructured fiber: fabrication and characterization. In: Optical fiber communication conference. Optical Society of America, p OWL6
51. De Hazan Y, MacChesney JB, Stockert TE, Trevor DJ, Windeler RS (2002) Sol gel method of making an optical fiber with multiple apetures. Google Patents
52. Kiang K et al (2002) Extruded single-mode non-silica glass holey optical fibres. Electron Lett 38(12):546–547
53. Hasan M, Habib MS, Habib MS, Razzak SA (2014) Highly nonlinear and highly birefringent dispersion compensating photonic crystal fiber. Opt Fiber Technol 20(1):32–38
54. Suzuki K, Kubota H, Kawanishi S, Tanaka M, Fujita M (2001) Optical properties of a low-loss polarization-maintaining photonic crystal fiber. Opt Express 9(13):676–680
55. Buczynski R (2004) Photonic crystal fibers. Acta Physica Polonica Series A 106(2):141–168
56. Buczynski R, Szarniak P, Pysz D, Kujawa I, Stepien R, Szoplik T (2004) Double-core photonic crystal fiber with square lattice. Photonic Cryst Mater Nanostruct 5450:223–230
57. Couny F, Roberts PJ, Birks T, Benabid F (2008) Square-lattice large-pitch hollow-core photonic crystal fiber. Opt Express 16(25):20626–20636
58. Falkenstein P, Merritt CD, Justus BL (2004) Fused preforms for the fabrication of photonic crystal fibers. Opt Lett 29(16):1858–1860

Publisher's Note